Research Article | Vol. 27, No. 7 | 1 Apr 2019 | OPTICS EXPRESS 10022
Optics EXPRESS

Low-threshold organic lasing from a square optical microcavity fabricated by imaging holography

WENBIN HUANG,[1] YAN-HUA LIU,[1,4] KE LI,[2] YAN YE,[1] DONG XIAO,[2] LINSEN CHEN,[1] ZHI-GANG ZHENG,[3] AND YAN JUN LIU[2,5]

[1]*School of Optoelectronic Science and Engineering & Collaborative Innovation Center of Suzhou Nano Science and Technology, Soochow University, Suzhou 215006, China*
[2]*Department of Electrical and Electronic Engineering, Southern University of Science and Technology, Shenzhen 518055, China*
[3]*Department of Physics, East China University of Science and Technology, Shanghai 200237, China*
[4]*yhliu@suda.edu.cn*
[5]*yjliu@sustc.edu.cn*

Abstract: We propose and demonstrate the versatile fabrication of optical subwavelength microcavities by using imaging holography. As a demonstration, a peculiar square optical microcavity with a periodicity of 400 nm is imaged from a micrometer-scale diffractive optical element, attributing to the interference by the refocusing of the multiple diffractive beams. By spin-coating an active conjugated polymer onto the microcavity, highly directional laser emission with a low pumping threshold of 0.5 kW/cm^2 is achieved. The effect of the film thickness on the lasing performance is also investigated. This imaging holography technique can enable convenient and easy fabrication of optical microcavities with subwavelength features, hence providing significant flexibility and richness on engineering the optical response of photonic nanostructures.

1. Introduction

Optical microcavities have been widely used to control the flow of photons and investigate the light-matter interactions in a tightly confined space. Microrings or microspheres, with size features in micrometers, could support total light reflections at the inner or outer surface and circulated standing waves are formed when the whispering gallery mode condition is fulfilled for certain wavelengths, exhibiting great potential in in microlasers and sensitive sensors [1]. Photonic crystals (PC) or photonic quasi-crystals (PQCs) are consisted of subwavelength features with some kind of ordering, i.e., the former has both translational invariance and rotational symmetry while the latter has only rotational symmetry. Such subwavelength ordering opens the bandgap for these microcavities, in which photons at specific wavelengths are prohibited, allowing for effective control over photon propagation or confinement [2]. When comparing the two types of microcavities, the microring or the microsphere with the feature size being one order larger is easier to fabricate, however, the PC or the PQC has obvious advantages in performance, including better optical confinement, higher wavelength sensitivity and more possibility for on-chip integration. As a result, PCs or PQCs have been exploited in various practical applications, such as mirrorless lasers, frequency filters, absorption-free mirrors, sharp-bend waveguides, or aberration-free negative refractive index lenses [3–5].

Due to the excellent optical effects of the PCs and PQCs, Purcell factor in these subwavelength microcavities is largely enhanced. When optical emitters are placed in them, a significant suppression of spontaneous emission can be achieved, opening a route for low-threshold and even thresholdless laser resonance [6]. In addition, these small-mode volume cavities could be an ideal platform for on-chip coherent light sources, which hold great

#358400 https://doi.org/10.1364/OE.27.010022
Journal © 2019 Received 23 Jan 2019; revised 18 Mar 2019; accepted 19 Mar 2019; published 26 Mar 2019

Optics EXPRESS

potential for various applications including on-chip optical communications and data-processing, lab-on-chip sensing and advanced displays [7]. As a result, mirrorless lasing is a very important application area for subwavelength microcavities and has aroused great interests from broad research fields [1,3]. To date, various PC or PQC microcavity lasers have been demonstrated, such as using periodic lines [8,9], circular gratings [10], square lattice PCs [11,12], triangular or hexagonal lattice PCs [13–16], cubic lattice PCs [17], Fibonacci PQC lines [18], Penrose PQCs [19] and dodecahedron PQCs [20]. Either the propagating photonic bandgap edge effect or the localized defect mode effect could stimulate laser emission [21]. Novel designs of optical microcavities with strong light confinement effects not only provide insights into the light-matter interactions but also new configurations for tiny coherent light sources.

Several approaches have be developed to fabricate these optical microcavities and corresponding microlasers, and they could be mainly classified into three categories. The first approach is through high-resolution direct write techniques [19–21], this can be implemented using either high-weight particles, such as the electron beam and the focused ion beam, or photons with specified techniques, such as the multi-photon absorption [22] and ultralow one-photon absorption [23]. 1D periodic or aperiodic subwavelength lines and 2D PC or PQC cavities with different lattice configurations have been demonstrated. It is even able to provide 3D PC cavities when combined with two triaxial piezoelectric stages [17]. The direct-write approach is potentially applicable to construct arbitrary optical microcavities, however these techniques are commonly time-consuming and usually only apply for small area fabrication, which limits their use mainly for scientific research purposes. The second approach is through interference lithography or holographic lithography. This technique utilizes several coherent beams to construct periodic or quasi-periodic light patterns and light-responsive materials function as the media to record the pattern. It is applicable to large area fabrication with a suitable expansion of the beam diameter. In addition, it could provide high-quality subwavelength structures with a sufficiently high resolution of 0.25λ. 1D, 2D and 3D PC microlasers have be frequently demonstrated using this technique [24]. Theoretically, all five 2D and fourteen 3D Bravais lattice structures could be formed with three and four coherent laser beams, respectively [25]. Furthermore, five-, seven-, and nine-fold symmetry PQCs are fabricated by interfering five, seven and nine coherent beams, respectively [26]. However, fabrication of PC or PQC microcavities with holographic lithography becomes increasingly difficult as the number of interfering laser beams increases. Properties of each laser beam including the polarization state, the incident angle and the phase delay should be precisely controlled. The third approach is based on self-assembly of colloidal particles or soft materials. For example, 3D PC cavities could be constructed by the infiltration of opal templates through self-assembly [27]. 1D and 3D PC cavities have also been demonstrated by the self-assembly of liquid crystals into cholesteric helical structures and blue phase structures, respectively [28]. Although PC cavities from self-assembly techniques are very cost-effective and potentially applicable to centimeter-scale areas, it is difficult to control the microcavity patterns on demand. In addition, the self-assembled structure quality is very sensitive to environmental parameters. Defects or distorted lines are usually inevitable, which significantly deteriorate microcavity laser performance. Therefore, it is highly desirable to develop a technique that could fabricate high quality PC or PQC microcavities with excellent flexibility and high efficiency.

In this work, we propose and demonstrate the versatile fabrication of optical microcavities using imaging holography. The resulted optical microcavity with subwavelength patterns can be viewed as a direct demagnified image from the diffractive optical element (DOE) with micrometer scale patterns. As a demonstration, we have designed and fabricated a particular square optical microcavity with four-fold symmetry, which consists of subwavelength periodic lines in x-y plane. By spin-coating a conjugated polymer as the active gain material, highly directional laser emission with an ultralow pumping threshold of 0.5 kW/cm^2 is

achieved. Microcavity laser properties including the divergence angle and wavelength tuning are also investigated. The imaging holographic technique is both efficient and flexible in providing optical microcavities with desired architectures, adding fruitful interest to the field of nanophononics.

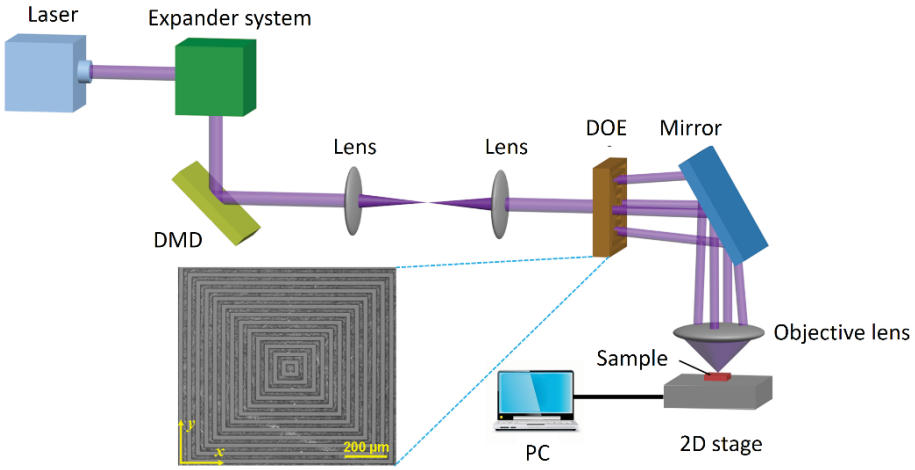

Fig. 1. Schematic illustration of the experimental setup of the imaging holography. The magnified inset shows the microscopic image of the DOE used in this work.

2. Experimental details

2.1 Subwavelength square microcavity fabrication using imaging holography

Figure 1 schematically illustrates the experimental setup for the proposed imaging holography technique. The laser beam (Advanced Optowave Corporation; Polarization: TE; Wavelength: 351 nm; Repetition rate: 1 kHz) is first collimated and expanded by the expander system, and then was directed to impinge on the digital micromirror device located before a 4*f* imaging system. The imaged writing beam is then diffracted into multiple beams by the DOE. The period of the DOE is designed to be far beyond the writing wavelength. As a result, the diffraction angles of the beams are sufficiently small which allow for the full collection by the objective lens. It should also be noted that only ± 1st orders are employed and the DOE depth is optimized to eliminate the 0th diffraction. At the imaging plane, these diffracted beams are focused by the objective lens, yielding the structured light field for microcavity fabrication. Theoretically, the light field at the image plane is a twice Fourier transformation of the DOE's transmission, which is merely influenced by the aberration of the lens. We have further carried out calculations (Refer to the Appendix) and find the generated light pattern at the image plane is a demagnified pattern of the DOE (demagnification 2M), where M is the magnification of the object lens and this is the reason why we refer to this technique as imaging holography. As a simple example, if the DOE is a low spatial frequency 1D grating with a period of 40 μm and the magnification of the objective lens is 50 × , then the final interference pattern is a 1D grating with a period of 400 nm, entering the optical subwavelength regime.

It is worth to mention that the theoretical derivation is general and applicable to the two-dimensional case. As the widely available laser direct write technique could fabricate arbitrary low spatial frequency DOEs, the imaging holography technique proposed here could provide various kinds of subwavelength patterns, depending on the requirements of practical applications. The imaging holography equation is not infinitely correct and we have further derived the resolution of the imaging holography technique to be $\lambda/4NA$, where λ is the lasing

Optics EXPRESS

wavelength and *NA* is the numerical aperture of the objective lens. In this work, we have utilized an objective lens with a *NA* of 0.85, leading to a theoretical lower-limit of the linewidth around 110 nm. The 2D computer-controlled stage could precisely distribute the subwavelength patterns on the photoresist with an error of 100 nm. As a result, the technique provides a method to generate structured light illumination for subwavelength microcavity fabrication and the lithography system could expose thousands of frames per second, featuring ultra-high efficiency for large-area fabrication. When compared with the traditional lithography technique for optical subwavelength microcavity fabrication, the imaging holography here shows much higher fabrication efficiency as compared to electron beam lithography, as it writes the one pattern in one laser pulse. When compared with the interference lithography technique, we do not need to precisely manipulate the parameters of each coherent beam while still benefiting from a flexibility in obtaining various kinds of subwavelength patterns.

In order to improve the optical confinement effect of the microcavity to behave as an efficient laser resonator, we have tried to fabricate a square optical microcavity which has never been reported before. This particular square microcavity lacks translational symmetry and has a four-fold rotational symmetry. For this purpose, the low spatial frequency square DOE was designed with line periods along x- and y-directions being 40 μm. In order to experimentally realize it, we first wrote the low spatial frequency pattern into the photoresist via the laser direct write equipment (iGrapher, SVG Optronics) and then transferred the pattern into the silica via reactive ion etching. The depth of the trenches was etched to be around 380 nm to eliminate the 0th-order transmission of the DOE at the operating wavelength. The inset in Fig. 1 shows the microscopic image of the obtained DOE, consisting of periodically distributed squares with a linewidth of 20 μm (200 nm error) and a spacing of 20 μm (200 nm error). In order to image the micrometer-scale DOE pattern into the optical subwavelength regime, we have employed an objective lens with a magnification of 50 × and a numerical aperture of 0.95. According to the above investigation, a square microcavity consisting of periodic squares with a linewidth of 200 nm and a spacing of 200 nm could be formed at the imaging plane, giving rise to the periodicity in both directions being 400 nm. The illuminated DOE size was 4 mm and the size of single imaged microcavity was 40 μm. The 2D stage moved with a step distance of 40 μm in x- and y-directions in accordance with laser exposure triggering to fill the substrate with repeated square optical microcavites.

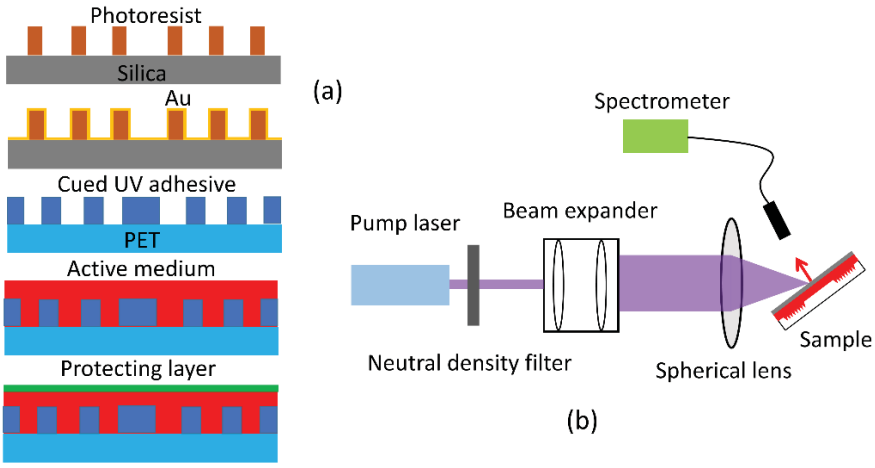

Fig. 2. (a) Schematic illustration of the preparation process of the square microcavity laser; (b) Optical setup for pumping and characterizing the microcavity laser.

Optics EXPRESS

2.2 Preparation and characterization of the square microcavity laser

The preparation process of the square microcavity laser is shown in Fig. 2(a). After exposure by the imaging holography system, the sample with the positive photoresist was immersed in the developer, which yields the relief pattern in the photoresist. A thin layer of gold nanoparticle (~5 nm) was then evaporated onto the photoresist to reduce the surface energy, enabling the use of the pattered photoresist as the mold for UV nanoimprinting. A drop of the UV adhesive was placed between the mold and the PET substrate, followed by a uniform UV exposure, providing the reverse square pattern in the cured adhesive after demolding. A thin organic semiconductor film consisting of the blue-emitting Poly (9, 9-dioctylfluorene) (PFO) conjugated polymer and the red-emitting Poly [2-methoxy-5-(2-ethylhexyloxy)-1, 4-phenylenevinylene] (MEH-PPV) one was spin-coated onto the substrate from the toluene solution (1.2 wt. %) as the gain medium. The two conjugated polymers serve as a Forster energy transfer system, in which PFO is the host material for light absorption and MEH-PPV is the guest material for light emission. The film thickness can be adjusted through the mixing ratio between MEH-PPV and PFO polymers since they have very different molecular weights (MEH-PPV: ~200 000, PFO: ~20 000). To prevent the performance degradation from oxygen and moisture, an additional polyvinyl alcohol layer (~200 nm) was spin-coated onto the active gain film. This encapsulation layer will also make the light mode distribution inside the gain layer more symmetric, leading to better laser performance. Figure 2(b) depicts the setup for optical excitation, the pump laser beam (Spectral Physics; working wavelength: 349 nm; pulse width: 8 ns; Polarization: S-polarized) was expanded and focused onto the sample into a spot with a diameter of 0.5 mm. Emission normal to the sample surface was collected and analyzed using a fiber-coupled spectrometer (Avaspec, spectral resolution: 0.19 nm) which was replaced with a high sensitivity energy meter (Coherent, J-10SI-HE) when the determination of the absolute output emission energy is required. The far-field emission patterns at different distances were recorded with a charge coupled device camera.

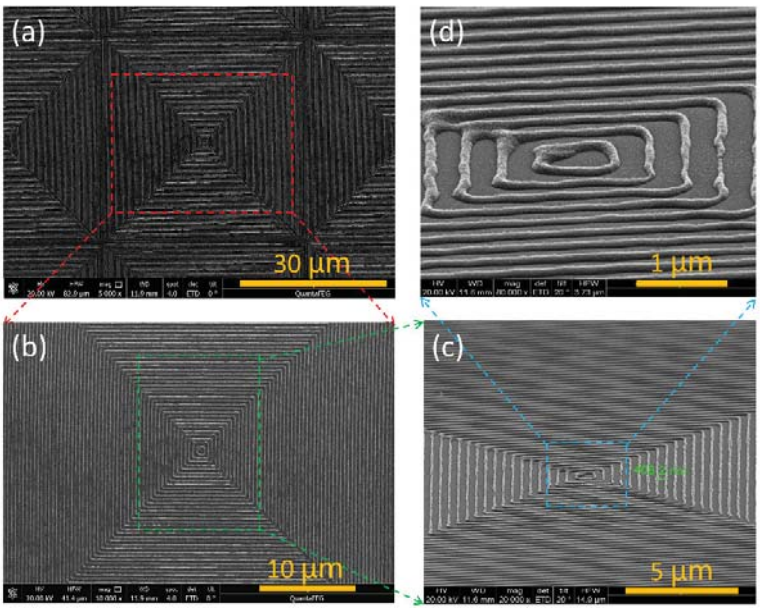

Fig. 3. SEM images of the square optical microcavity at different magnifications.

3. Results and discussion

3.1 Subwavelength square optical microcavity

Figure 3 shows the scanning electron microscope (SEM) images of the recorded subwavelength pattern on the photoresist. The total patterned area was 1 cm2 and the imaging holography system could complete the writing in ~5 mins. From Fig. 3(a), the size of each optical microcavity is around 40 μm. They are stitched together to form the whole structure and the stitching error is around 100 nm, which is attributed to the control stage. The microcavity pattern lacks translational symmetry while has a four-fold rotational symmetry. In previous 2D PC or PQC structures, distributed dots with translational or rotational order constitute the microcavity in similar with atoms taking the place of the crystal lattice [2]. The particular microcavity in this work could be regarded as a combination of the 1D grating with the 2D square-lattice PC. As a result, we term this structure as square optical microcavity and it is expected to support pseudogaps for effective light confinement. Figures 3(b)-3(d) show more morphological details of the square optical microcavity at high SEM magnifications. The measured periodicities of ~400 nm in x and y directions agree well with the theoretical prediction. The linewidth and spacing of the squares are about 120 nm and 280 nm, respectively. These microcavity parameters deviate from the theoretical calculation due to the development conditions. The interference quality of the diffracted beams might deteriorate slightly at boundaries due to the stitching error, subsequently inducing non-uniformity and minor distortions at these locations. Overall, the experimental results confirmed the excellent capability of our imaging holography technique in fabricating high-quality subwavelength optical microcavities. As mentioned in Sec. 2.1, the subwavelength pattern is a demagnified image of the low spatial frequency DOE, which means this technique is applicable to various kinds of microcavites with periodicities along specific directions. The square optical microcavity is just a simple example for the demonstration of the feasibility of the imaging holography technique.

3.2 Lasing performance

Figure 4 presents emission spectra at different pumping intensities that were collected normal to the sample surface. At a low pumping energy density of 3.5 $\mu J/cm^2$, the spectrum shows the typical spontaneous emission that mainly results from electronic emission band of MEH-PPV located at 575 nm and the vibronic side band at 630 nm. Although the emission spectrum below 550 nm is not shown here, it is worth noting that the characteristic emission band (locating at ~460 nm) from the host PFO polymer does not appear on the spectrum, indicating a complete Forster energy transfer from the host to the guest emitter. The emission behavior changes dramatically as the pumping intensity increases to 4.3 $\mu J/cm^2$. A sharp lasing peak at 618.8 nm with the bandwidth of 0.3 nm appears and dominates the spectrum with significant suppression of the emission bands at 570 nm and 630 nm. During the transition from the fluorescence to the laser action, it is not accompanied by the presence of ASE which may narrow itself at the shoulder band of the guest emitter. The narrow bandwidth confirms the laser action from the square optical microcavity, since the bandwidth of typical ASE exceeds 5 nm. It is also worth to note here, the bandwidth of the lasing peak may not be very accurate due to the limitation in the spectrometer resolution.

Optics EXPRESS

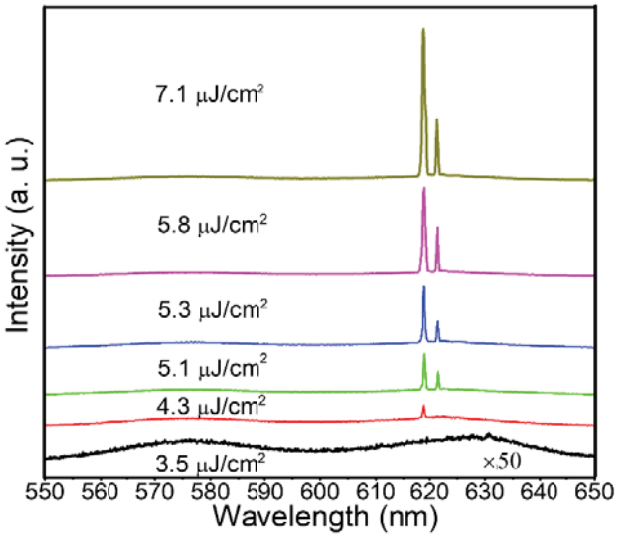

Fig. 4. Emission spectra from the square microcavity laser excited at different pump intensities.

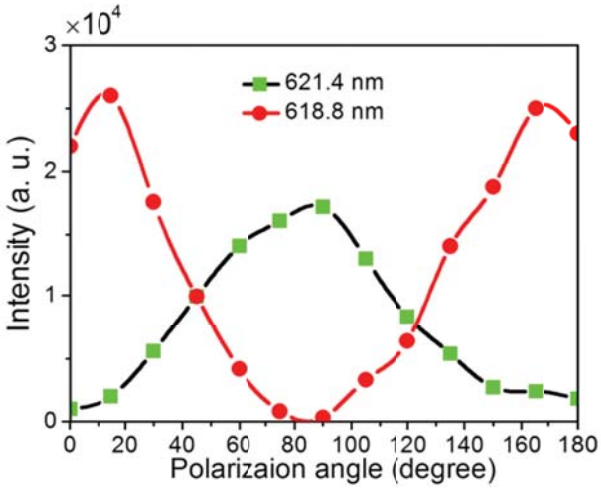

Fig. 5. Intensity dependence on the polarization angle for the lasing peak at 618.8 nm (the red circles) and 621.4 nm (the green squares).

With a further increase in the pumping intensity, a second lasing peak at 621.4 nm appears. The Bragg equation is written as $m\lambda = 2n_{eff}\Lambda$, where λ is the lasing wavelength, m is the Bragg order, n_{eff} is the effective refractive index of the mode and Λ is the periodicity. According to material suppliers, the refractive index of the active layer, the UV adhesive layer and the protecting layer is 1.76, 1.52 and 1.51 (at the wavelength of 620 nm), respectively, yielding an effective mode refractive index of 1.56 according to the waveguide theory. If the Bragg order is 2, one obtained the lasing wavelength of 624 nm which agrees well the experimental data. As there are two periodicities along the vertical and parallel directions, the square optical microcavity supports distributed feedback in both directions. In addition, since the periodicities in two direction may be slightly different, this square microcavity could emit dual lasing, which is already observed in the emission spectra shown in Fig. 4. In order to further confirm this, we have analyzed the intensity dependence of the

two lasing peaks on the polarization angle when transmitting through a linear polarizer (Fig. 5). It is clear that one lasing peak is TE polarized while the other is TM polarized, demonstrating the orthogonal distributed feedback in this square optical microcavity.

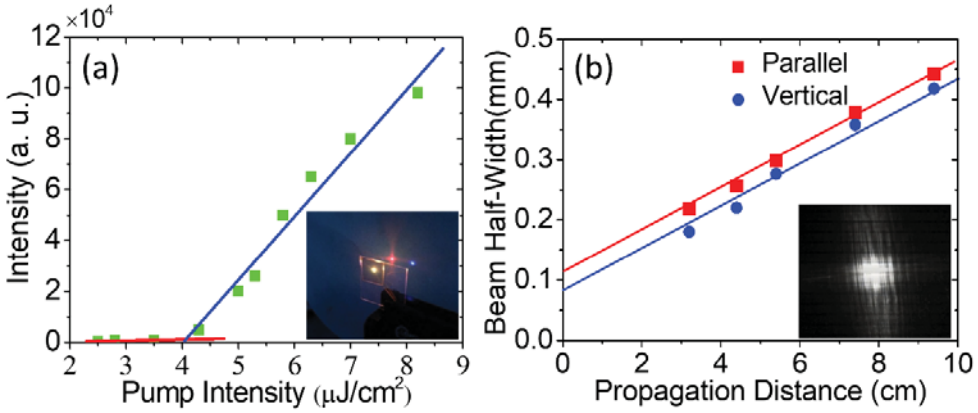

Fig. 6. (a) Emission intensity as a function of pump intensity, and the inset shows the image of the directional laser emission normal to the sample surface; (b) Laser spot half-width as a function of the propagation distance. The inset shows a captured spot image.

Figure 6(a) shows the integrated emission intensity as a function of the pump intensity. When the pumping intensity is below the lasing threshold, the emission intensity increases slowly, implying the omnidirectional fluorescence regime. As the pump intensity is above the threshold, emission intensity increases abruptly, indicating the directional laser action. We could deduce the working threshold to be around 4 μJ/cm^2 which corresponds to a power density of 0.5 kW/cm^2. In comparison, a square lattice PC laser with the PFO polymer as the gain medium showed a lasing threshold of 3 kW/cm^2 where the cavity is written by high-resolution electron beam lithography [11], while an even higher threshold of 150 kW/cm^2 was demonstrated by directly recording the square lattice PC structure into the polymer film [12], indicating the superiority of this particular square optical microcavity over the typical square-lattice PC as laser resonators. We further measured the energy of the laser emission from the square optical microcavity using the high sensitivity energy meter and found the absolute slope efficiency is around 8.0%, making it a comparatively efficient microlaser. The inset in Fig. 6(a) shows the photograph of the laser emission. It is normal to the sample surface and energy is highly concentrated in the central spot. Lasing resonating in the sample plane was outcoupled to the sample normal by the square microcavity. The periodicity would exert a Bragg vector on the original wave vector of lasing, which couples it into the free space with a new wave vector. The outcoupling process is independent of the feedback process. According to the momentum conservation equation, and m' is the grating coupling order:

$$\frac{2\pi}{\lambda}\sin(\theta) = \pm\frac{2\pi n_{eff}}{\lambda} \pm m'\frac{2\pi}{\Lambda} \tag{1}$$

According to the above investigation, the second Bragg ordered lasing wavelength is related with the periodicity via $\lambda = n_{eff}\Lambda$. Put this into the coupling equation, we have:

$$\sin(\theta) = (\pm 1 \pm m')n_{eff} \tag{2}$$

Restricted by $|\sin(\theta)| \le 1$, m' can only take the value of 1, thus we have $\sin(\theta) = 0$, which means lasing is coupled out of the waveguide to the cell normal, in accordance with the experimental result.

We further investigated the divergence properties of the laser emission by directly collecting the optical signal into a camera at different distances. The dependence of the beam half-width on the propagation distance is shown in Fig. 6(b), and the inset in Fig. 6(b) shows a captured image. The observed spot images are well localized and the divergence half-angle in both directions is estimated to be around 5 mrad, which is comparable to that from the square lattice PC polymer laser [11]. This observation implies that the lasing action is resulted from the feedback of the periodic structure in the long-range regime, forming well-defined extended modes spreading coherently throughout the microcavity. These modes are diffracted by the reciprocal lattice points of the square microcavity structure, giving rise to standing waves that provide strong feedback in both directions. At higher pumping densities, the highly directional laser spot evolves into a more divergent cross profile, which consists of two pairs of opposite arc lines lying in the parallel and vertical directions. The cross-shape profile emission indicates the inherent existence of linearly polarized transverse modes resulting from ± 1-order Bragg modes in both directions, further confirming that the feedback in this particular cavity is a coherent summation of two orthogonal periodic gratings [29].

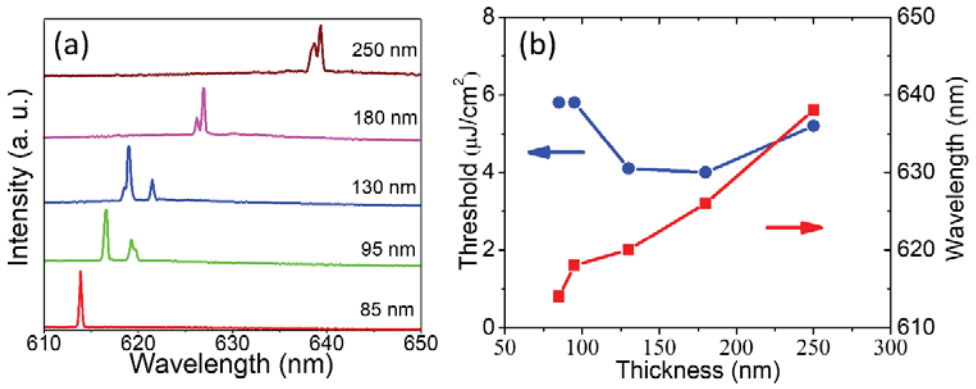

Fig. 7. Lasing performance of samples with different active film thicknesses: (a) emission spectra, (b) lasing threshold and wavelength.

3.3 Lasing tunability

As a further step into the reliability of this square optical microcavity, we have fabricated polymer lasers with different active film thicknesses. By changing the weight ratios between MEH-PPV and PFO from 1:10 to 4:10, we can adjust the blended active film thickness from 85 nm to 250 nm. Figure 7 shows the lasing spectra above the thresholds from these samples. We can clearly see that the lasing wavelength shifts from 613 nm to 638 nm as the active film thickness increases. This could be mainly attributed to the increase of the effective refractive index when the active film becomes thick [11]. The lasing wavelength shift shows a nearly linear trend, as shown in Fig. 7(b) from 613 nm to 638 nm. The lasing peaks from different samples remain narrow within the range of 0.3 nm to 0.8 nm. Some additional peaks are present due to the periodicity nonuniformity over the whole microcavity during DOE fabrication. The dependence of the lasing wavelength on the film thickness could be explained using the waveguiding theory [30]. The high refractive index active layer was sandwiched between the substrate and the protecting layer with low refractive indices, constituting a planar waveguide structure. The lasing wavelength depends on the effective refractive index of the supported mode in the waveguide which increases quasi-linearly with the active film thickness. Figure 7(b) also shows the dependence of the lasing threshold on the

active film thickness. It is the lowest when the film thickness is between 130 nm and 170 nm. When the film is too thin, optical confinement deteriorates, resulting in a decrease in optical gain for each loop. When the film is too thick, the shallow corrugations are insufficient for efficient feedback. In addition, the optical gain coefficient also varies within and out of the range of the ASE peak, which subsequently affects the lasing thresholds as well. Overall, the lasing threshold falls between 0.5 kW/cm^2 and 0.75 kW/cm^2 in the whole wavelength range, indicating excellent lasing performance.

4. Conclusion

In conclusion, we have demonstrated an efficient, reliable and versatile approach called imaging holography to fabricate optical microcavities. A square optical microcavity with subwavelength lines has been fabricated and is imaged directly from a micrometer-scale DOE pattern. High-performance polymer lasers with low threshold, narrow bandwidth, and high directivity have been realized by spin-coating the conjugated polymer film onto this peculiar microcavity. With this technique, various kinds of structured light illumination could be generated via the replacement of the low frequency DOE, giving rise to efficient fabrication of different subwavelength microcavities, which adds a great freedom in designing new optical microcavities for effective light modulation.

Appendix – Theoretical investigation of the imaging holography technique

Figure 1 shows the experimental setup for the imaging holography technique. A laser is coupled with an expander to generate a collimated light beam which incidents normally toward the Fourier transform system. The Fourier transform system is based on a 4-f optical configuration, in which a DOE is placed at the image plane of the system. The DOE's spatial frequency is low enough to ensure its period far beyond the illuminating lasing wavelength, and the depth is optimized to eliminate the 0th order transmission. Then the interference pattern by ±1 diffractions is projected by a tube lens and demagnified by an objective lens, whereby the pattern and the focal plane of the objective lens meet the object image conjugation relationship. Therefore, at the image plane of the objective lens, the demagnified interference pattern is produced for instantly structured illumination. In addition, the interference pattern size is determined by the size of the DMD image and the magnification of the objective lens.

Theoretically, the light field at the image plane is a twice Fourier transform of the DOE's transmission, and it can be expressed in Fourier series:

$$t(x_0, y_0) = \sum_{m=-\infty}^{m=+\infty} \sum_{n=-\infty}^{n=+\infty} C_m C_n \exp\left(j2\pi f_{mx_0} x_0 + j2\pi f_{ny_0} y_0\right) \tag{3}$$

where m and n are the diffraction orders, C_m and C_n are the constant amplitudes, and f_{mx0} and f_{ny0} are the m^{th}- and n^{th}-order frequencies of the DOE, respectively. Only ± 1th-order diffracted beams are utilized in and the generated light field at the imaging plane can be written as:

$$1\,U(x, y) = C\left[\exp\left(j2\pi f_x x + j2\pi f_y y\right) + \exp\left(-j2\pi f_x x - j2\pi f_y y\right)\right] \tag{4}$$

At the imaging plane of the objective lens, (f_x, f_y) becomes (Mf_{1x0}, Mf_{1y0}), and M is the magnification of the objective lens. The intensity distribution is further expressed as:

$$I(x, y) = \left|U(x, y)\right|^2 = C_0 + C_1\left[\exp\left(j4\pi f_x x + j4\pi f_y y\right) + \exp\left(-j4\pi f_x x - j4\pi f_y y\right)\right] \tag{5}$$

Which indicates that the generated light pattern at the image plane is a demagnified pattern of the DOE (demagnification 2M), and as a result the spatial frequency becomes ($2Mf_{1x0}$, $2Mf_{1y0}$). With this method, various kinds of structured light illumination could be generated via the replacement of the low frequency DOE, giving rise to efficient fabrication

of different subwavelength microcavities. It should also bear in mind that arbitrary low frequency DOE could be fabricated using the widely available laser direct write technique.

Funding

National Natural Science Foundation of China (NSFC) (Grant Nos. 61505131, 61575132, 61822504 and 51873060), the Natural Science Foundation of Jiangsu Province (Grant No. BK20181166), China Postdoctoral Science Foundation (Grant No. 2017T100403), the National Science Foundation of the Jiangsu Higher Education Institutions of China (No. 18KJB510040), Natural Science Foundation of Guangdong Province (Grant No. 2017A030313034), and Shenzhen Science and Technology Innovation Council (Grant No. JCYJ20170817111349280).

References

1. L. He, Ş. K. Özdemir, and L. Yang, "Whispering gallery microcavity lasers," Laser Photonics Rev. **7**(1), 60–82 (2013).
2. J. D. Joannopoulos, P. R. Villeneuve, and S. Fan, "Photonic crystals: putting a new twist on light," Nature **386**(6621), 143–149 (1997).
3. Y. Akahane, T. Asano, B.-S. Song, and S. Noda, "High-Q photonic nanocavity in a two-dimensional photonic crystal," Nature **425**(6961), 944–947 (2003).
4. A. Mekis, J. C. Chen, I. Kurland, S. Fan, P. R. Villeneuve, and J. D. Joannopoulos, "High Transmission through Sharp Bends in Photonic Crystal Waveguides," Phys. Rev. Lett. **77**(18), 3787–3790 (1996).
5. A. Arie and N. Voloch, "Periodic, quasi-periodic, and random quadratic nonlinear photonic crystals," Laser Photonics Rev. **4**(3), 355–373 (2010).
6. V. S. C. Manga Rao and S. Hughes, "Single quantum-dot Purcell factor and β factor in a photonic crystal waveguide," Phys. Rev. B Condens. Matter Mater. Phys. **75**(20), 205437 (2007).
7. M. T. Hill and M. C. Gather, "Advances in small lasers," Nat. Photonics **8**(12), 908–918 (2014).
8. Y. J. Liu, X. W. Sun, P. Shum, H. P. Li, J. Mi, W. Ji, and X. H. Zhang, "Low-threshold and narrow-linewidth lasing from dye-doped holographic polymer-dispersed liquid crystal transmission gratings," Appl. Phys. Lett. **88**(6), 061107 (2006).
9. C. Karnutsch, C. Pflumm, G. Heliotis, J. C. deMello, D. D. C. Bradley, J. Wang, T. Weimann, V. Haug, C. Gärtner, and U. Lemmer, "Improved organic semiconductor lasers based on a mixed-order distributed feedback resonator design," Appl. Phys. Lett. **90**(13), 131104 (2007).
10. G. A. Turnbull, A. Carleton, G. F. Barlow, A. Tahraouhi, T. F. Krauss, K. A. Shore, and I. D. W. Samuel, "Influence of grating characteristics on the operation of circular-grating distributed-feedback polymer lasers," J. Appl. Phys. **98**(2), 023105 (2005).
11. G. Heliotis, R. Xia, G. A. Turnbull, P. Andrew, W. L. Barnes, I. D. W. Samuel, and D. D. C. Bradley, "Emission characteristics and performance comparison of polyfluorene lasers with one- and two-dimensional distributed feedback," Adv. Funct. Mater. **14**(1), 91–97 (2004).
12. T. Zhai, X. Zhang, Z. Pang, and F. Dou, "Direct writing of polymer lasers using interference ablation," Adv. Mater. **23**(16), 1860–1864 (2011).
13. B. Ellis, M. A. Mayer, G. Shambat, T. Sarmiento, J. Harris, E. E. Haller, and J. Vuckovic, "Ultralow-threshold electrically pumped quantum-dot photonic-crystal nanocavity laser," Nat. Photonics **5**(5), 297–300 (2011).
14. M.-K. Seo, K.-Y. Jeong, J.-K. Yang, Y.-H. Lee, H.-G. Park, and S.-B. Kim, "Low threshold current single-cell hexapole mode photonic crystal laser," Appl. Phys. Lett. **90**(17), 171122 (2007).
15. M. Meier, A. Mekis, A. Dodabalapur, A. Timko, R. E. Slusher, J. D. Joannopoulos, and O. Nalamasu, "Laser action from two-dimensional distributed feedback in photonic crystals," Appl. Phys. Lett. **74**(1), 7–9 (1999).
16. D. Luo, X. W. Sun, H. T. Dai, Y. J. Liu, H. Z. Yang, and W. Ji, "Two-directional lasing from a dye-doped two-dimensional hexagonal photonic crystal made of holographic polymer-dispersed liquid crystals," Appl. Phys. Lett. **95**(15), 151115 (2009).
17. A. Tandaechanurat, S. Ishida, D. Guimard, M. Nomura, S. Iwamoto, and Y. Arakawa, "Lasing oscillation in a three-dimensional photonic crystal nanocavity with a complete bandgap," Nat. Photonics **5**(2), 91–94 (2011).
18. L. Mahler, A. Tredicucci, F. Beltram, C. Walther, J. Faist, H. E. Beere, D. A. Ritchie, and D. S. Wiersma, "Quasi-periodic distributed feedback laser," Nat. Photonics **4**(3), 165–169 (2010).
19. M. Notomi, H. Suzuki, T. Tamamura, and K. Edagawa, "Lasing action due to the two-dimensional quasiperiodicity of photonic quasicrystals with a penrose lattice," Phys. Rev. Lett. **92**(12), 123906 (2004).
20. S.-K. Kim, J.-H. Lee, S.-H. Kim, I.-K. Hwang, Y.-H. Lee, and S.-B. Kim, "Photonic quasicrystal single-cell cavity mode," Appl. Phys. Lett. **86**(3), 031101 (2005).
21. H. Altug and J. Vucković, "Photonic crystal nanocavity array laser," Opt. Express **13**(22), 8819–8828 (2005).
22. J. K. Hohmann, M. Renner, E. H. Waller, and G. von Freymann, "Three-dimensional μ-printing: an enabling technology," Adv. Opt. Mater. **3**(11), 1488–1507 (2015).
23. M. T. Do, T. T. N. Nguyen, Q. Li, H. Benisty, I. Ledoux-Rak, and N. D. Lai, "Submicrometer 3D structures fabrication enabled by one-photon absorption direct laser writing," Opt. Express **21**(18), 20964–20973 (2013).

Optics EXPRESS

24. Y. J. Liu and X. W. Sun, "Electrically tunable three-dimensional holographic photonic crystal made of polymer-dispersed liquid crystals using a single prism," Jpn. J. Appl. Phys. **46**(10A), 6634–6638 (2007).
25. G. P. Crawford, "Holographic photonic crystals," Opt. Eng. **43**(9), 1973–1987 (2004).
26. S. P. Gorkhali, J. Qi, and G. P. Crawford, "Switchable quasi-crystal structures with five-, seven-, and ninefold symmetries," J. Opt. Soc. Am. B **23**(1), 149–158 (2006).
27. M. Scharrer, A. Yamilov, X. Wu, H. Cao, and R. P. H. Chang, "Ultraviolet lasing in high-order bands of three-dimensional ZnO photonic crystals," Appl. Phys. Lett. **88**(20), 201103 (2006).
28. H. Coles and S. Morris, "Liquid-crystal lasers," Nat. Photonics **4**(10), 676–685 (2010).
29. G. A. Turnbull, P. Andrew, W. L. Barnes, and I. D. W. Samuel, "Operating characteristics of a semiconducting polymer laser pumped by a microchip laser," Appl. Phys. Lett. **82**(3), 313–315 (2003).
30. W. B. Huang, Z. H. Diao, L. S. Yao, Z. L. Cao, Y. G. Liu, J. Ma, and L. Xuan, "Electrically tunable distributed feedback laser emission from scaffolding morphologic holographic polymer dispersed liquid crystal grating," Appl. Phys. Express **6**(2), 022702 (2013).